From latent space to voxel-wise quantification of dermis fibrous network in LC-OCT images

Raoul Missodey[1,2], Sylvie Treuillet[1], Remy Leconge[1], Yves Lucas[1], Samuel Ralambondrainy[2], Jean-Hubert Cauchard[2], and Franck Bonnier[2]

[1] Laboratoire PRISME, Polytech Orléans, 12 rue de Blois, 45067 Orléans, France
`raoul.missodey@etu.univ-orleans.fr`
[2] LVMH Recherche, 185 avenue de Verdun, 45800 Saint Jean de Braye, France
`fbonnier@research.lvmh-pc.com`

Abstract. It is well established that the effects of skin aging, with visible manifestations such as loss of elasticity, wrinkle formation, and changes in firmness, are primarily linked to structural and mechanical changes associated with alterations in the extracellular matrix of the dermis, involving collagen and elastin fibers. Breakdown of these fibers leads to changes in their organization, characterized by decreased density and increased anisotropy. While deep learning models have demonstrated strong performance in age prediction from Line-field Confocal Optical Coherence Tomography (LC-OCT) images, their "black box" nature limits interpretability regarding which structural features drive predictions.

For explainability attempt, this study bridges the latent space of a 3D ResNet-18 deep learning model trained for age prediction on LC-OCT images and the quantitative characterization of collagen on a multi-ethnic dataset of healthy female volunteers aged 20 to 70 years.

Principal Component Analysis followed by Hierarchical Clustering of the final global average pooling layer features revealed three distinct clusters corresponding to age-related collagen organization patterns, rather than the five chronological age groups used for training. An improved curve enhancement method combining Orientation Field Transform with fuzzy logic system feature aggregation was developed, enabling voxel-wise extraction of dermis fibrous network density and dominant orientation metrics. Results demonstrate strong agreement between this metrics and deep learning identified clusters: the cluster corresponding to the young age group [20-30] exhibits higher fiber density and isotropic orientation, while the cluster corresponding to the old age group [50-70] shows a decrease in density and an increase in anisotropy. This work establishes that deep learning models implicitly learn interpretable dermis fibrous characteristics, and provide a framework for explainable automated analysis of dermal aging in LC-OCT imaging.

Keywords: LC-OCT imaging · Dermis fibrous network · Orientation field transform · Latent space.

1 Introduction

Collagen and elastin, the main structural proteins in the dermal extracellular matrix of the skin are affected by aging processes that result in reduced elasticity, compromised strength, and visible signs of cutaneous aging. As the dermis matures, the once abundant, tightly packed and well-organized collagen [10] undergo progressive fragmentation and disorganization, transitioning from an isotropic network into a more anisotropic arrangement [23, 25]. This structural deterioration is caused by a decrease in the production of new collagen and an accumulation of advanced glycation end-products, which together weaken the tissue's mechanical strength [9]. Detecting these specific subcutaneous modification, such as subtle variations in local fiber orientation and density, remains a significant challenge in conventional histology. Consequently, there is a growing need for automated quantification methods capable of resolving these complex morphological features at a granular level, moving beyond simple scoring to a precise, pixel-wise characterization of the aging matrix.

Traditionally, the characterization of dermis fibrous network has relied on either qualitative assessment by expert pathologists or semi-quantitative techniques. Despite being the clinical standard, expert visual evaluation is subjective and susceptible to differences in interpretation among observers, making it inadequate for detecting subtle, sub-visual shifts in fiber organization over large tissue area. Conversely, early computational methods utilizing Fourier transforms or edge-detection filters often struggle with the complex, intertwined nature of dermis fibrous network, frequently sacrificing local spatial resolution for global texture statistics [12, 16]. Image quality also plays a strong role in this analysis. Some techniques for dermis fibrous network visualization and characetrization such as MultiPhoton Microscopy (MPM), Optical Coherence Tomography (OCT), Reflectance Confocal Microscopy (RCM) present limitations regarding depth of penetration and resolution. Line-field Optical Coherence Tomography (LC-OCT) is a new non invasive high resolution ($\sim 1\mu m$) imaging technique which can acquire vertical, horizontal and 3D images down to $500\mu m$ in the skin [5].

With the advent of deep learning (DL), image analysis has been revolutionized, offering access to powerful tools for tissue characterization tasks. Our previous work established that a 3D ResNet-18 model achieves accurate age prediction from LC-OCT dermis images with a mean absolute error (MAE) of 4.2 years [2], confirming that these images contain age-discriminative information. However, a significant gap remains in the interpretability and granularity of DL models. Most deep learning approaches operate as "black boxes", mapping input images directly to class labels without explicitly modeling the underlying structural parameters that drive these predictions.

Understanding the interpretability of DL models in this context serves two important purposes : firstly, it provides scientific validation that the model learns biologically meaningful features. Secondly, it enables translation of learned representations into quantitative metrics. In this paper, it is hypothesized that, by leveraging the latent space of deep learning models, it can be demonstrated that model predictions are strongly correlated with the learned features.

The contributions of this work are threefold:

- We analyse the features in the latent space of a 3D ResNet-18 model trained for age prediction on a multi ethnic dataset of skin LC-OCT images, using dimensionality reduction and hierarchical clustering methods.
- We propose a more robust method to extract fibers in images based on fuzzy logic that better preserves their continuity.
- We demonstrate that the fiber density and their dominant orientation exhibit strong agreement with the clusters identified in the latent space of the DL model.

The following section summarizes the relevant work. The proposed methods for collagen fiber characterization are presented in section 3. The experimental results are discussed in section 4, before concluding.

2 Related work

2.1 Explanaible AI for skin imaging

As the use of black-box deep learning models has rapidly expanded, explainable artificial intelligence (XAI) has emerged to provide insights into their decision making processes. Methods such as Grad-CAM [19] and Integrated Gradients [21] produce spatial attribution maps indicating which image regions influence a prediction. In histopathology, such explanation maps have been used to identify relevant tissue structures and uncover dataset biases [8]. However, these maps can produce misleading attributions and, by themselves, indicate the relevance of image regions without demonstrating that the network relies on human-interpretable biological concepts [17]. Concept-based methods such as TCAV address this limitation by quantifying a model's sensitivity to predefined, human-interpretable concepts [11].

2.2 Analysis of dermis fibers

Approaches based on image transforms

The first works for quantification of collagen organization relied heavily on signal processing techniques. Methods based on the Fast Fourier Transform (FFT) have been widely used to extract dominant fiber orientation and anisotropy from image patches [1, 16]. Such methods smooths out local variations and reduces spatial resolution, making them less effective where fibrous network architecture changes rapidly over short distances. CurveAlign and CT-FIRE represent standard toolboxes that utilize curvelet transforms and fiber tracking algorithms to quantify individual fiber geometry [3, 4]. While effective for extracting statistics such as fiber alignement, length, width, angle... from high-contrast images (such as Second Harmonic Generation microscopy), these methods often lack extraction of curvy or varying thickness fibers. Another approach consists in enhancing the fibrous network in the image by using vessel enhancement methods such as Frangi filter [7], Sato filter [18] or also Hessian based methods [13] which are strongly dependent on the choosed scale range.

Approaches based on deep learning

Park et al. [14] introduced a framework for collagen fiber centerline tracking in fibrotic tissue. Their approach incorporates a Variational AutoEncoder (VAE) to generate synthetic centerlines with controllable topological properties, which are then translated into realistic training images via a conditional Generative Adversarial Network (cGAN). This use of VAE-based synthetic training data enables the precise tracking of fiber centerlines and the subsequent quantification of morphological features such as orientation, alignment, and length without relying solely on limited annotated biological datasets. Recent studies have also demonstrated the ability of CNNs to analyse collagen fiber organisation in Hematoxylin & Eosin (H&E) stained slides. Pham et al. [15] introduced a Universal Convolutional Neural Network (UCNN) designed to be histology-independent, effectively classifying scar tissue and characterizing fiber organization across both H&E and Masson's Trichrome stained images. By leveraging feature maps from the network's convolutional layers, their method automatically extracts quantitative metrics such as collagen density and directional variance. This work showed that CNN trained on collagen images for classification task learned simultaneously features such as density or alignement. Our work investigates if the classification of the network is in agreement with the same tendancy when extracting quantitative metrics such as density and alignement from computational methods.

3 Methods

3.1 Latent space scanning for dermis fibrous network characterization

A 3D ordinal regression ResNet-18 model was previously developed to predict facial dermis age from LC-OCT images. Detailed information on the model development can be found in [2]. Differences in the dermis fibrous network can be observed according to two main properties: density and alignment of fibers in this network. The latter is closely related to orientation information. Given that the model was trained exclusively on dermis fibrous network images, we hypothesize that its strong performance derives from learning structural features such as fiber density, orientation, length, or waviness as a function of age. The primary objective of this part is to investigate whether the learned features in the model's latent space correspond to biologically meaningful fibrous network organization, and whether these patterns align with known age-related structural changes. While the DL model was trained to predict five discrete age groups ([20-30], [31-40], [41-50], [51-60], [61-70]), the dermis aging may not follow these arbitrary chronological boundaries. Unsupervised clustering of latent features allows natural groupings to emerge based on structural similarity, potentially revealing distinct phases of collagen degradation. The final global average pooling layer (GAPL) of the 3D ResNet-18 architecture contains a 512-dimensional feature vector that represents a highly compressed representation of the input data and captures the most critical information. Based on that vector and to reduce its dimensionality, a Principal Component Analysis (PCA) was first applied to the 512 features of the GAPL, reduced to the 50 principal components which capture 99.91% of the cumulative explained variance. Subsequently, a Hierarchical Clustering Analysis (HCA) was performed on the reduced 50-dimensional feature space to cluster these features into 'n' classes based on a dendrogram analysis. For visualizing clusters within high-dimensional data, 2D PCA map and t-distributed Stochastic Neighbor Embedding (t-SNE) was used.

The subsequent phase of the fiber organization characterization involves performing voxel-wise information extraction from the LC-OCT images of these clusters. This step is essential to assess the correlation between the quantitative voxel-wise metrics and the clustered features. By analyzing this correlation, we aim to validate that the deep learning model effectively captures the characteristics of dermis fibrous network, thereby confirming the model's accuracy and reliability in characterizing fiber organization.

3.2 Voxel-wise dermis fibrous network quantification

An improved curve enhancement method, based on the approach developed by Yeung et al. [26] was applied. The method started by measuring at voxel level, the strength of oriented lines passing through a sphere with radius r. Let $L_I(x,d)$ be the strength of a line oriented in direction d and centered at voxel x in image I;

$$L_I(x,d) = \int_{-r}^{r} I(x+sd)\,ds \tag{1}$$

where $d \in \bar{V}^3$ the set of unit vectors in half of the discretised 3D Euclidean space [26]. Following that, a primary orientation field can be generated by :

$$OF(x) = \left\{ \max_{d\in\bar{V}^3} L_I(x,d),\ \arg\max_{d\in\bar{V}^3} L_I(x,d) \right\} \tag{2}$$

whose elements are respectively the strength and direction. The alignment of the orientation field along the direction d can be quantified by the dot product:

$$AO(x,d) = \int_{-r}^{r} \max_{d\in\bar{V}^3} L_I(x+sd,d)(2(\arg\max_{d\in\bar{V}^3} L_I(x+sd,d).d)^2 - 1)ds \tag{3}$$

and the 3D orientation field transform takes the maximum value of the alignment with respect to d in each pixel:

$$OFT(x) = \max_{d \in \bar{V}^3} AO(x, d) \tag{4}$$

In [26], Yeung et al found that relying solely on the maximum of L_I to detect 3D curves structures is insufficient, as it falsely identifies point-like objects that generate high values across multiple directions. The authors stated that, unlike isotropic blobs, real curves exhibit significant variability in integral magnitude depending on the orientation. Therefore, they replaced the max by the mean and absolute deviation in OF in order to better separate curves from noise or point structures and measure the variability. The overall method provides 6 features :

$$F_1(x) = \max_{d \in \bar{V}^3} L_I(x, d); \tag{5}$$

$$F_2(x) = \frac{1}{|\bar{V}^3|} \sum_{d \in \bar{V}^3} L_I(x, d); \tag{6}$$

$$F_3(x) = \frac{1}{|\bar{V}^3|} \sum_{d \in \bar{V}^3} |F_2(x) - L_I(x, d)|\,; \tag{7}$$

$$F_4(x) = OFT(x); \tag{8}$$

$$F_5(x) = \frac{1}{|\bar{V}^3|} \sum_{d \in \bar{V}^3} AO(x, d); \tag{9}$$

$$F_6(x) = \frac{1}{|\bar{V}^3|} \sum_{d \in \bar{V}^3} |F_5(x) - AO(x, d)|\,; \tag{10}$$

In order to detect curves in the 3D images, Yeung et al. proposed to multiply some of the features [26]. We propose here to apply a fuzzy logic method to combine these features and better highlight the fibers while preserving their linear continuity. A fuzzy system architecture [24, 27] is typically characterized by four distinct components : the fuzzifier, the rules base, inference engine and the defuzzifier, as depicted in Fig. 1. The fuzzifier transforms crisp numerical inputs into linguistic variables, such as Low, Medium, and High, through Gaussian, sigmoid, trapezoidal, or triangular shape. Subsequently, the inference engine processes these fuzzified inputs by applying a set of IF-THEN rules stored in the rule base to derive the appropriate response. In the final step, the defuzzifier converts the aggregated fuzzy output back into a scalar value. The centroid method is commonly used to produce the final output of the system

The proposed methodology processed features from OF and OFT separately. The specific instantiation of the four components is detailed below :

Fuzzifier: The features F_1, to F_6 are normalized and transformed into three linguistic terms (Low, Medium, and High) using the following polynomial spline-based functions:

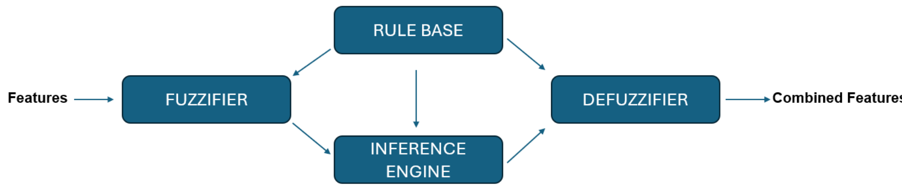

Fig. 1. A fuzzy system architecture.

- Low : Modeled using a Z-shaped function,

$$\mu_Z(x;a,b) = \begin{cases} 1, & x \le a, \\ 1 - 2\left(\dfrac{x-a}{b-a}\right)^2, & a < x \le \dfrac{a+b}{2}, \\ 2\left(\dfrac{b-x}{b-a}\right)^2, & \dfrac{a+b}{2} < x < b, \\ 0, & x \ge b. \end{cases} \tag{11}$$

- Medium : Modeled using a Triangle-shaped function,

$$\mu_{tri}(x;a,b,c) = \max\left(\min\left(\frac{x-a}{b-a}, \frac{c-x}{c-b}\right), 0\right) \tag{12}$$

- High : Modeled using an S-shaped function,

$$\mu_S(x;a,b) = \begin{cases} 0 & x \le a \\ 2\left(\frac{x-a}{b-a}\right)^2 & a < x \le \frac{a+b}{2} \\ 1 - 2\left(\frac{b-x}{b-a}\right)^2 & \frac{a+b}{2} < x < b \\ 1 & x \ge b \end{cases} \tag{13}$$

where a, b, c are empirical parameters.

Rule Base and Inference Engine : For each linguistic output level $\ell \in \{\text{Low}, \text{Medium}, \text{High}\}$, the activation strength is obtained by the union (OR) of the corresponding memberships across the three input features:

$$\alpha_\ell(x) = \max\Big(\mu_\ell(F_1(x)),\ \mu_\ell(F_2(x)),\ \mu_\ell(F_3(x))\Big), \tag{14}$$

so that a strong response from any single feature is sufficient to activate that level. Because the activation is computed by this continuous aggregation rather than by selecting discrete rules, every input combination is handled uniformly: a voxel with mixed memberships (e.g. F_1 Low, F_2 Medium, F_3 High) simultaneously activates all three levels in proportion to its degrees of membership, and the final probability is their weighted blend. The same procedure is applied independently to F_4, F_5, F_6 for the OFT stream.

Defuzzifier: To ensure computational efficiency suitable for large 3D volumes, a singleton-based defuzzification method (similar to a Zero-Order Takagi-Sugeno model [20]) is applied to obtain an output probability.

Global Aggregation: The system runs two parallel fuzzy inference streams (features F_1, F_2, F_3 from OF, and features F_4, F_5, F_6 from OFT). The intuition behind this method is that the OF features act like a high scale filter. The final result is calculated by multiplying the normalized crisp outputs of each streams.

This method makes it easy to obtain information about the density and length of the dominant orientation of the region of interest (dermis volume). The density ρ is calculated by dividing the number of extracted fibers by the image size. The dominant orientation ($\overrightarrow{DO}$) can be calculated using directional statistics [6] as :

$$\overrightarrow{DO} = \frac{1}{n}\left(\sum_i u_i, \sum_i v_i, \sum_i w_i\right) \tag{15}$$

where (u_i, v_i, w_i) represents the maximal oriented vector at voxel i. If the magnitude of $\overrightarrow{DO}$ is close to 1, the fibers predominantly follow a preferred direction; if, on the contrary, it is close to 0, they have different orientations.

4 Experiments and results

4.1 Data

The multiethnic dataset includes 325 female volunteers, evenly distributed between Caucasian, Asian, and African-American skin tones. About 20 women were recruited in each age group [20-30], [31-40], [41-50], [51-60], [61-70] for each dataset. Images were collected as part of a study on the effectiveness of cosmetic products. Consequently, only healthy cases are included here. For each volunteer, nine hundred LC-OCT images of 1200 $\times$ 500 $\times$ 350 voxels were acquired using a DeepLive$^{\text{TM}}$ system (DAMAE Medical, France) on three different facial zones (temple, cheekbone and mandible). Three acquisitions were performed for each area. Both vertical images (B-scans) and horizontal ones (C-scans) have a spatial resolution of $\sim$1 μm per pixel. The dimensions of the dermis fiber region of interest used in the experiment have a shape of 1200 $\times$ 500 $\times$ 128 as described in [2].

4.2 Latent space feature clustering

Three 3D ResNet-18 models were trained on each ethnic group (A-Caucasian, B-Asian, C-African American) for age prediction. Next, we analyse the features in the latent space using dimensionality reduction and hierarchical clustering methods. The clustering was applied to the PCA-projected latent features using Ward linkage and euclidean distance. This choice favors compact clusters by minimizing the increase in within cluster variance during agglomeration. The analysis of the dendrogram and PCA projections suggested a consistent structure with three clusters across Caucasian and Asian ethnic groups; therefore, the dendogram was cut to obtain three clusters.

For the caucasian dataset, the DL age prediction model yielded a MAE = 4.2 years, showing a strong correlation with the chronological age. Fig. 2A illustrates the projection of the last AGPL features of the model on the first two principal components. This two components capture 83,40% of variance meaning, a significant portion of the information present in the extracted features. The different colors in the plot stand for the five age groups. It shows clusters of points, which may correspond to groups of similar samples. On the left of the center, a cluster of ∼50 to ∼70 years old (y.o) indicate that there is a similar pattern in the organization of dermis fibrous network in both age groups [51-60] and [61-70] even if the ∼50 to ∼70 is not provided to the model as one single class. On the rigth a cluster is also formed specifically corresponding to young group ∼20 to ∼30 y.o. On the contrary, there is a random distribution from ∼30 to ∼50 y.o where there is no specific cluster but a continuous variation with age; the fibrous network of the dermis begins to deteriorate more or less quickly depending on the volunteers.

According to the dendrogram analysis illustrated in Fig. 3A, three clusters can be identified after tree cutting. Cluster 1 contains 37 volunteers, 20 of whom are in the [20- 30] age group. Cluster 2 contains 22 volunteers, with 21 in the [30-50] age group, and Cluster 3 contains 41 volunteers, 38 of them belonging to the [50-70] age group. As a visualization technique, t-SNE allows the latent space to be linked to a two-dimensional visual map while preserving natural clusters in the data. In Fig. 3B, according to the partition provided by the dendrogram, the colored points are relatively well-separated clusters. However some overlap can be observed for the cluster 2 (green points), suggesting a greater dispersion of dermis fibrous network alteration in the middle-aged volunteers. These clustering results suggest that the model has learned to group samples based on collagen organization patterns that correlate with chronological age groups, but are not identical to it.

For the Asian dataset, the MAE was slightly higher (5.1 years). The latent space organization obtained was very close to the one observed in the case of Caucasian dataset with the two components capturing 87,14% of variance. Similarly, the plot indicates three clusters but with less clear separation between age groups (Fig. 2B). For example the cluster formed of ∼20 to ∼30 y.o on the right is mixed with volunteers aged 30 to 40 y.o. 0n the left of the center of the plot also, the cluster of ∼50 to ∼70 y.o contains volunteers aged between 40 and 50 years. These results illustrate that Asian skin generally appears younger than its chronological age.

The dendrogram analysis (Fig. 3B) helps also identify three clusters with the following characteristics : Cluster 1 contains 31 volunteers, 22 of whom are in the [20- 30] age group. Cluster 2 contains 52 volunteers, with 33 in the [30-50] age group, and Cluster 3 contains 26 volunteers, 25 of whom are in the [50-70] age group. This model well separates more structured dermis fiber and desorganised dermis fiber while putting together all other images corresponding to fiber transformation process.

For African-American dataset, the MAE was the highest (6.5 years). The variance of the latent space features is explained at 81,96% by the first two components (Fig. 2C). The cloud is much less well separated than for the two previous ethnic groups, showing a less efficient prediction model. The drop in the model accuracy and latent space organization could be due to biological factors or phototype-related limitations of imaging. In particular, melanin is more present in dark skin, and its higher refractive index weakens the signal in the dermis [22].

However the dendrogram analysis (Fig. 3C) also identifies three clusters: Cluster 1 contains 22 volunteers, 10 of whom are in the [20-30] age group. Cluster 2 contains 46 volunteers, with 24 in the [30-50] age group, and Cluster 3 contains 48 volunteers, 32 of whom are in the [50-70] age group.

To validate that the clusters formed in each model latent space, reflect true structural differences, we carry out a quantitative analysis of the fibers in the next section.

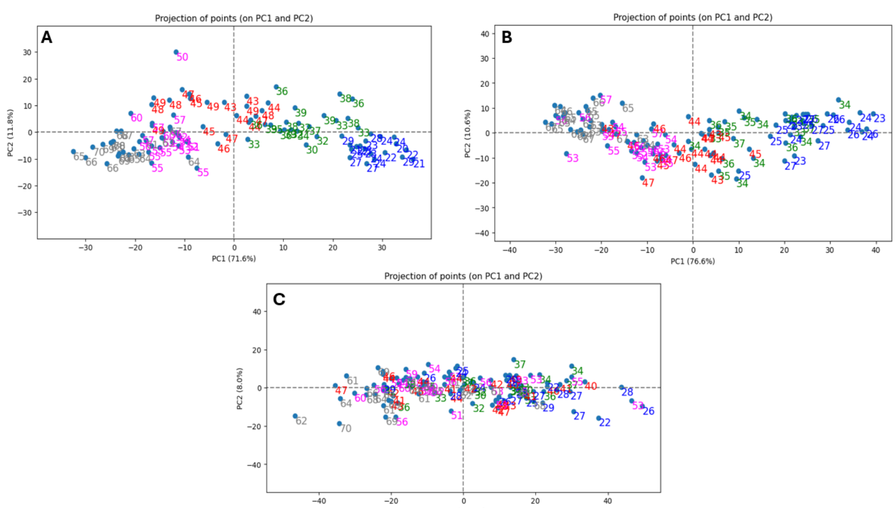

Fig. 2. Projection of latent features onto the first two principal components for each ethnic group: A- Caucasian, B- Asian, C- African American. Volunteers are color-coded according to their age.

4.3 Fiber isolation from LC-OCT images

The proposed approach was applied on all dermis fiber ROI with a sphere radius of $r = 7$ voxels. This value of r was fixed based on the average lateral diameter

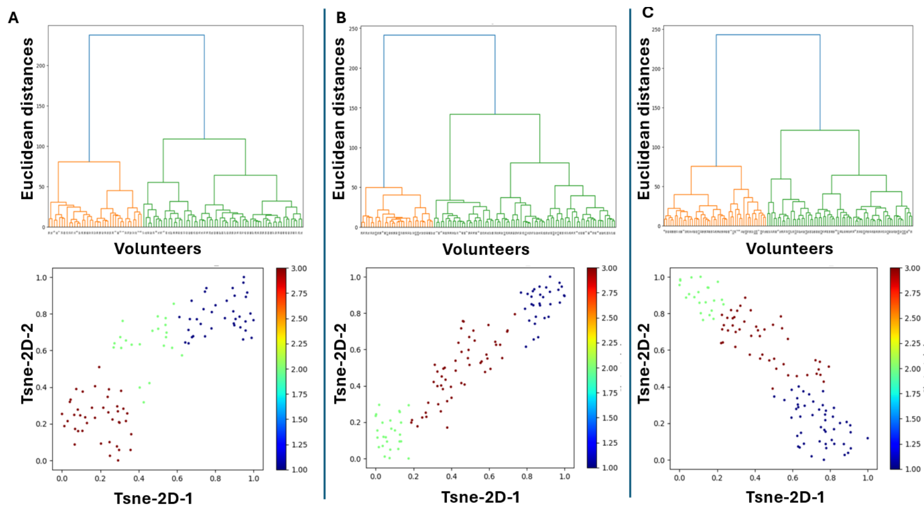

Fig. 3. First row: the dendrogram analysis (the height of the branches indicates the dissimilarity between the merged groups); second row : 2D projection of the clustering performed by t-SNE. The three ethnic groups are distributed on the columns (A- Caucasian, B- Asian, C- Affrican American.

of the fibrous network of 4-7 μm [2, 26]. Fig. 4 compares the proposed method to Yeung's method on an image of a 21 y.o caucasian woman on cheekbone. It can be seen that the fuzzy method yields higher extraction of dermis fibrous network compared to the simple pixel-wise multiplication aggregation proposed by Yeung et al. [26].

It can be observed that applying gamma correction with $\gamma = 0.2$, voxel-wise multiplication as proposed by Yeung, acts like keeping higher intensity values while our proposed fuzzy method extracts correctly dermis fibrous network.

Fig. 5 outlines its density and dominant orientation based on the formulas defined previously.

The analysis of the dermis fibrous network revealed distinct age-related trends across the three different ethnic groups. Regarding network density, the Caucasian cohort exhibited statistically significant differences (Figure 5A) between the three clusters identified by the dendrogram ($ANOVA : p < 0.001$). A clear separation is evident between Cluster 1 (younger group, median $\rho = 34.6$) and Cluster 3 (older group, median $\rho = 29.4$), supporting the hypothesis that density drops with age. Cluster 2 which includes individuals aged approximately 30 to 50 years, (middle group, median $\rho = 32.5$) displayed a significantly higher variance, linked to the biological processes developing inside this age range, in which dermis fibrous network density begins to deteriorate more or less rapidly. Furthermore, these findings align with the predictions generated by the DL models, as visualized in the PCA projection (Figure 2A). Similar significant age-related degradation was observed in the African-American cohort ($ANOVA : p < 0.001$), with

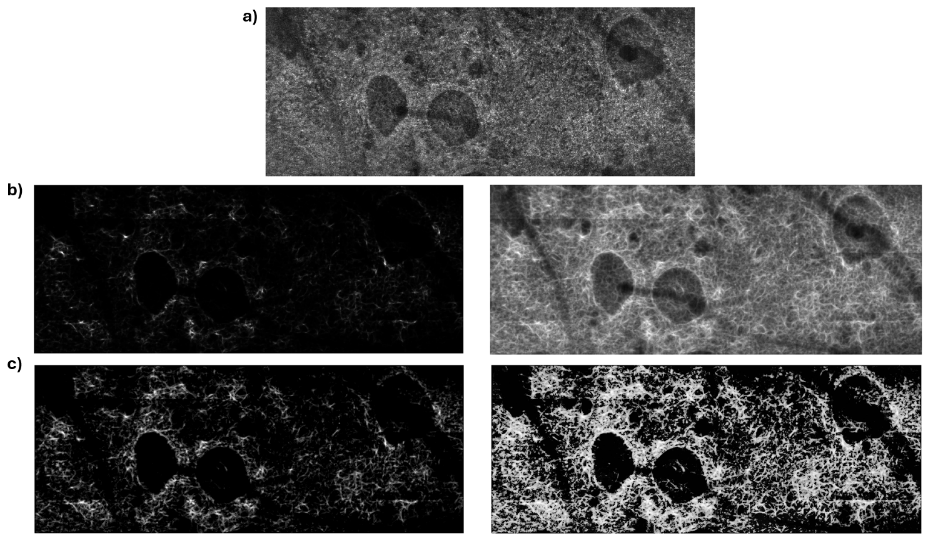

Fig. 4. Dermis fiber extraction : a) Raw 2D horizontal LC-OCT collagen image of 21 y.o caucasian female volunteer on cheekbone. b) Dermis fibrous network isolation using Yeung's method (left) and after contrast enhancement by gamma correction (right). c) Dermis fibrous network isolation using our proposed fuzzy method (left) and after contrast enhancement by gamma correction (right).

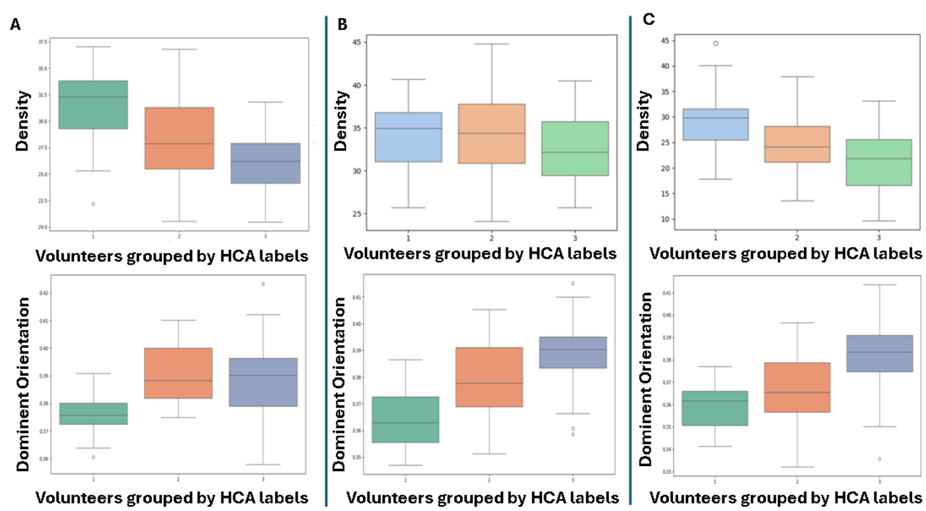

Fig. 5. By columns for the three ethnic groups: A-Caucasian, B-Asian, C-African American: on the first line, the distribution fiber density according to the 3 groups identified by dendrogram; on the second line, the distribution of the dominant fiber orientation according to the same 3 groups.

density dropping from a median $\rho = 29.7$ in Cluster 1 to $\rho = 21.3$ in Cluster 3 (Figure 5B). In contrast, while the Asian cohort demonstrated a similar downward trend (Figure 5C) between clusters (medians $\rho = 34.9, 34.4$ and 32.5 for Clusters 1, 2, and 3, respectively), these differences did not reach statistical significance ($ANOVA : p = 0.142$)). This requires further investigation regarding the dendrogram analysis and the optimal number of clusters chosen.

Regarding the magnitude of the dominant orientation, as depicted in each second row of Figure 5, a highly consistent and statistically significant trend was observed across all three ethnic groups ($ANOVA : p < 0.001$ for each group). In all cohorts, Cluster 1 displayed the lowest values in the dominant orientation metrics (Caucasian: median $|\overrightarrow{DO}| = 0.372$; Asian: 0.363; African-American: 0.362). These lower values indicate a more isotropic data distribution, signifying that the fibrous network in younger individuals is randomly oriented and less structured. As age increases, this fibers are more and more aligned; older age groups (Clusters 2 and 3) consistently showed higher dominant orientation magnitudes across the Caucasian (0.384 and 0.382), Asian (0.378 and 0.390), and African-American (0.366 and 0.383) cohorts. This uniform increase suggests that structural realignment and stiffening of the dermal fibers with age is a universal phenomenon across the studied populations.

These metrics, calculated directly from voxel intensities, show strong agreement with the clustering observed in the latent feature space generated by deep learning. In the Caucasian and African-American cohorts, fiber density significantly decreased across the three latent-space clusters ($ANOVA : p < 0.001$ for both), while the magnitude of the dominant orientation significantly increased across clusters in all three cohorts ($ANOVA : p < 0.001$). The progressive decrease in density and the increase in the magnitude of fiber orientation are in accordance with the age-related groupings discovered by HCA, confirming that the 3D ResNet-18 model has implicitly taken into account these structural properties in his age predictions.

5 Conclusion

This study establishes a link between deep learning latent representations and quantifiable dermis fibrous network properties through 3D LC-OCT image processing. By analyzing the feature space of a 3D ResNet-18 model trained for age prediction in a multi-ethnic context, we identified three biologically meaningful clusters corresponding to distinct phases of dermal aging, rather than the five chronological age groups used during training.

Our fuzzy logic-based curve enhancement method improves voxel-wise extraction of density and dominant orientation of the dermis fibrous network that strongly corroborate the deep learning derived clusters. Specifically, younger individuals (20-30 years) exhibit dense, isotropically oriented fibers, while aged individuals (50-70 years) show reduced density and increased anisotropy, with intermediate ages (30-50 years) demonstrating high individual variability consistent with differential aging rates.

These findings support our intuition that deep learning models implicitly learn interpretable structural features, advancing model explainability in biomedical imaging. The accordance between latent space analysis and computational metrics provides both scientific insight into learned representations and practical methodology for explainable automated dermal aging assessment. Future work should incorporate additional fiber characteristics and validate our findings across diverse populations.

Ethics statement The study was approved by the French Ethics Committee "Comité de protection des personnes sud méditerranée I" (IDRCB : 2021-A00101-40). A written informed consent was obtained from all participants.

References

1. Alberini, R., Spagnoli, A., Sadeghinia, M.J., Skallerud, B., Terzano, M., Holzapfel, G.A.: Fourier transform-based method for quantifying the three-dimensional orientation distribution of fibrous units. Scientific Reports **14**(1), 1999 (2024)
2. Assi, A., Fischman, S., Lopez, C., Pedrazzani, M., Grignon, G., Missodey, R., Korichi, R., Cauchard, J.H., Ralambondrainy, S., Bonnier, F.: Evaluating facial dermis aging in healthy caucasian females with lc-oct and deep learning. Scientific Reports **14**(1), 24113 (2024)
3. Bredfeldt, J.S., Liu, Y., Conklin, M.W., Keely, P.J., Mackie, T.R., Eliceiri, K.W.: Automated quantification of aligned collagen for human breast carcinoma prognosis. Journal of pathology informatics **5**, 28 (2014)
4. Bredfeldt, J.S., Liu, Y., Pehlke, C.A., Conklin, M.W., Szulczewski, J.M., Inman, D.R., Keely, P.J., Nowak, R.D., Mackie, T.R., Eliceiri, K.W.: Computational segmentation of collagen fibers from second-harmonic generation images of breast cancer. Journal of biomedical optics **19**(1), 016007–016007 (2014)
5. Dubois, A., Levecq, O., Azimani, H., Siret, D., Barut, A., Suppa, M., Del Marmol, V., Malvehy, J., Cinotti, E., Rubegni, P., et al.: Line-field confocal optical coherence tomography for high-resolution noninvasive imaging of skin tumors. Journal of biomedical optics **23**(10), 106007–106007 (2018)
6. Fisher, N.I., Lewis, T., Embleton, B.J.: Statistical analysis of spherical data. Cambridge university press (1993)
7. Frangi, A.F., Niessen, W.J., Vincken, K.L., Viergever, M.A.: Multiscale vessel enhancement filtering. In: International conference on medical image computing and computer-assisted intervention. pp. 130–137. Springer (1998)
8. Hägele, M., Seegerer, P., Lapuschkin, S., Bockmayr, M., Samek, W., Klauschen, F., Müller, K.R., Binder, A.: Resolving challenges in deep learning-based analyses of histopathological images using explanation methods. Scientific reports **10**(1), 6423 (2020)
9. Haydont, V., Bernard, B.A., Fortunel, N.O.: Age-related evolutions of the dermis: Clinical signs, fibroblast and extracellular matrix dynamics. Mechanisms of ageing and development **177**, 150–156 (2019)
10. He, T., Fisher, G.J., Kim, A.J., Quan, T.: Age-related changes in dermal collagen physical properties in human skin. PLoS One **18**(12), e0292791 (2023)

11. Kim, B., Wattenberg, M., Gilmer, J., Cai, C., Wexler, J., Viegas, F., et al.: Interpretability beyond feature attribution: Quantitative testing with concept activation vectors (tcav). In: International conference on machine learning. pp. 2668–2677. PMLR (2018)
12. Nejim, Z., Navarro, L., Morin, C., Badel, P.: Quantitative analysis of second harmonic generated images of collagen fibers: a review. Research on Biomedical Engineering **39**(1), 273–295 (2023)
13. Ng, C.C., Yap, M.H., Costen, N., Li, B.: Automatic wrinkle detection using hybrid hessian filter. In: Asian Conference on Computer Vision. pp. 609–622. Springer (2014)
14. Park, H., Li, B., Liu, Y., Nelson, M.S., Wilson, H.M., Sifakis, E., Eliceiri, K.W.: Collagen fiber centerline tracking in fibrotic tissue via deep neural networks with variational autoencoder-based synthetic training data generation. Medical image analysis **90**, 102961 (2023)
15. Pham, T.T.A., Kim, H., Lee, Y., Kang, H.W., Park, S.: Universal convolutional neural network for histology-independent analysis of collagen fiber organization in scar tissue. IEEE Access **10**, 34379–34392 (2022)
16. Pijanka, J.K., Markov, P.P., Midgett, D., Paterson, N.G., White, N., Blain, E.J., Nguyen, T.D., Quigley, H.A., Boote, C.: Quantification of collagen fiber structure using second harmonic generation imaging and two-dimensional discrete fourier transform analysis: application to the human optic nerve head. Journal of biophotonics **12**(5), e201800376 (2019)
17. Plass, M., Kargl, M., Kiehl, T.R., Regitnig, P., Geißler, C., Evans, T., Zerbe, N., Carvalho, R., Holzinger, A., Müller, H.: Explainability and causability in digital pathology. The Journal of Pathology: Clinical Research **9**(4), 251–260 (2023)
18. Sato, Y., Nakajima, S., Shiraga, N., Atsumi, H., Yoshida, S., Koller, T., Gerig, G., Kikinis, R.: Three-dimensional multi-scale line filter for segmentation and visualization of curvilinear structures in medical images. Medical image analysis **2**(2), 143–168 (1998)
19. Selvaraju, R.R., Cogswell, M., Das, A., Vedantam, R., Parikh, D., Batra, D.: Gradcam: visual explanations from deep networks via gradient-based localization. International journal of computer vision **128**(2), 336–359 (2020)
20. Sugeno, M.: Industrial applications of fuzzy control. Elsevier Science Inc. (1985)
21. Sundararajan, M., Taly, A., Yan, Q.: Axiomatic attribution for deep networks. In: International conference on machine learning. pp. 3319–3328. PMLR (2017)
22. Ulrich, M., Lange-Asschenfeldt, S.: In vivo confocal microscopy in dermatology: from research to clinical application. Journal of biomedical optics **18**(6), 061212–061212 (2013)
23. Wang, H., Shyr, T., Fevola, M.J., Cula, G.O., Stamatas, G.N.: Age-related morphological changes of the dermal matrix in human skin documented in vivo by multiphoton microscopy. Journal of Biomedical Optics **23**(3), 030501–030501 (2018)
24. Wang, L.X., Mendel, J.M., et al.: Fuzzy basis functions, universal approximation, and orthogonal least-squares learning. IEEE transactions on Neural Networks **3**(5), 807–814 (1992)
25. Wu, S., Li, H., Yang, H., Zhang, X., Li, Z., Xu, S.: Quantitative analysis on collagen morphology in aging skin based on multiphoton microscopy. Journal of biomedical optics **16**(4), 040502–040502 (2011)
26. Yeung, W.T., Cai, X., Liang, Z., Kang, B.H.: 3d orientation field transform. Pattern Analysis and Applications **27**(1), 6 (2024)
27. Zadeh, L.A.: Fuzzy sets. Information and control **8**(3), 338–353 (1965)